

Paper:

Development of Autonomous Mobile Robot that Can Navigate in Rainy Situations

Naoki Akai*, Yasunari Kakigi**, Shogo Yoneyama**, and Koichi Ozaki**

*Institutes of Innovation for Future Society, Nagoya University
Furo, Chikusa, Nagoya, Aichi 466-8601, Japan
E-mail: akai@coi.nagoya-u.ac.jp

**Graduate School of Engineering, Utsunomiya University
7-1-2 Yoto, Utsunomiya, Tochigi 321-8585, Japan
E-mail: {kakigi@ir.ics, yoneyama@ir.ics, ozaki@cc}.utsunomiya-u.ac.jp
[Received January 20, 2016; accepted June 14, 2016]

The Real World Robot Challenge (RWRC), a technical challenge for mobile outdoor robots, has robots automatically navigate a predetermined path over 1 km with the objective of detecting specific persons. RWRC 2015 was conducted in the rain and every robot could not complete the mission. This was because sensors on the robots detected raindrops and the robots then generated unexpected behavior, indicating the need to study the influence of rain on mobile navigation systems – a study clearly not yet sufficient. We begin by describing our robot’s waterproofing function, followed by investigating the influence of rain on the external sensors commonly used in mobile robot navigation and discuss how the robot navigates autonomously in the rain. We conducted navigation experiments in artificial and actual rainy environments and those results showed that the robot navigates stably in the rain.

Keywords: autonomous mobile robot, Real World Robot Challenge, navigation in rainy situation, influence of rain against sensors

1. Introduction

The mission of the Real World Robot Challenge (RWRC) held annually in Japan since 2007 [1] is to have robots navigate a predetermined path over 1 km automatically and unaided by any environmental arrangements of human assistants. Robots must also detect specific persons during navigation. In the nine RWRCs held thus far, RWRC 2015 was the first to be conducted in the rain. Due to the rain, every robot could not complete the mission.¹ Almost all of the robots in RWRC 2015 had light detection and ranging (LIDAR), which frequently detected raindrops and caused the robots to act unexpectedly, e.g.,

1. Three robots achieved the navigation mission in RWRC 2015, but there were seven robots which achieved the navigation mission through past trial runs. Also, four robots completed the mission. These results indicate that rain reduces navigation function.

obstacle avoidance. Although our mobile robots [2, 3] completed missions in trial experiments, they could not do so in the rain. Clearly rain adversely influenced autonomous navigation significantly. Our objective in this study is thus to overcome the influence of rain and enable stable autonomous navigation in rainy situations.

Despite the many robots built to work in outdoor environments, e.g., [4–6], the waterproofing functions that have been discussed have not included the influence of rain on external sensors and robot performance, i.e., only considering waterproofing that prevented hardware problems.

Yamashita et al. focused on the camera observation of raindrops falling on the camera screen and succeeded in reducing the rain’s influence [7]. Insofar as we know, no research has investigated how rain influences other external sensors, e.g., LIDAR or magnetic sensors. Sonar and LIDAR are used for underwater exploration [8, 9], but we have focused on rain rather than underwater conditions.

We start by discussing the robot’s waterproofing. We developed this robot in a previous study [2], finding that its waterproofing function was insufficient because raindrops hit the light receptors of sensors. We thus produced additional eaves by using a 3D printer that gave us the flexibility to produce forms attachments easily mounted on the robot. We also investigated the influence of rain on the external sensors commonly used in mobile robot navigation and discuss how our robot conducted autonomous navigation in the rain. After implementing the above items on our robot, we conducted navigation experiments in artificial rain and confirmed that the robot navigates stably in the rain.

2. Prerequisite

2.1. Mobile Robot

Figure 1 shows the robot used in this study. Our robot, shown in **Fig. 1**, has three types of external sensors, i.e., LIDAR UTM-30LX, camera Logicool C910, and magnetic sensor 3DM-DH and has an outer cowl. LIDARs



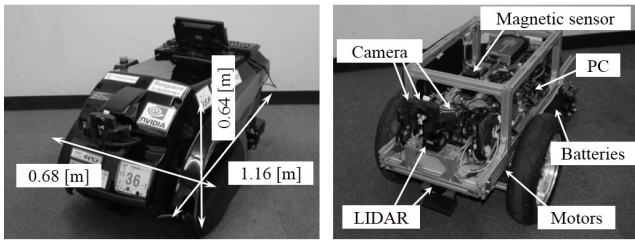


Fig. 1. Mobile robot.

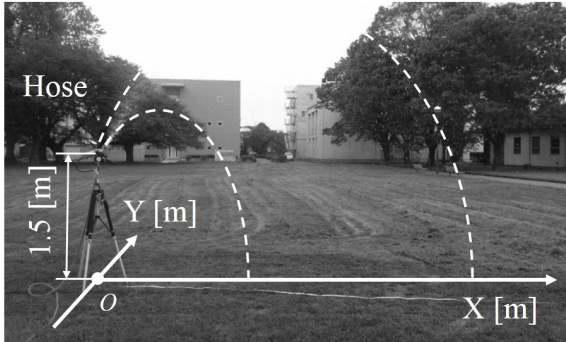


Fig. 2. "Artificial" showers.

are used for localization, avoiding obstacles, and detecting specific persons. Cameras are used only for detecting specific persons. The magnetic sensor is used for localization [3]. Although the cowl blocks almost all raindrops, some raindrops intrude from LIDAR and camera clearances and sometimes become attached to sensor light receptors. To help prevent these raindrop problems, we added additional eaves produced by using 3D printers as detailed in the next section.

2.2. Artificial Rainy Condition

The rain conditions under which RWRC 2015 was conducted resembled those of an evening shower, i.e., precipitation at 10 to 30 mm/h. Our experience suggested that such strong rain influenced only mobile robot navigation.² Since rain similar to such showers is rare, we approximated similar conditions by using a hose.

Figure 2 shows our artificial "rainy" conditions. Hose flow was set to 0.00033 m³/s and the hose was left at 1.5 m above the ground. GR20GNF produced by Green Life [a] was used as a nozzle set to "full." The shower was diffused about 4 m by reaching to the ground as shown in Fig. 3. Precipitation averaged about 20 mm/h and the angles between an orthogonal line to the ground and line that water drops followed were under 30°. Although our "rainy" conditions were not ideal, sensors similar to those we saw at RWRC 2015 were sufficient for our evaluation.

2. We conducted some navigation experiments in rainy day in which precipitation is approximately from 1 to 3 mm/h, but strong influence did not appear. We will describe about the experiments at Section 6.

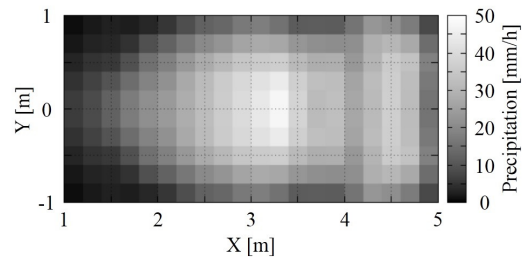


Fig. 3. Shower precipitation distribution. Coordinates are shown in Fig. 2.

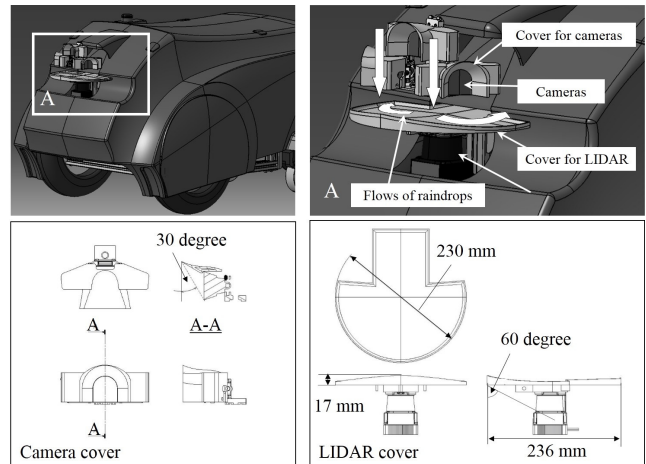


Fig. 4. Eaves parts for the sensors and expected raindrop flows.

3. Hardware Design for Waterproofing

Cameras and LIDAR cannot measure precisely when raindrops become attached to light receptors. Exterior and inner shapes of a robot are important to preventing water intrusion and hardware problems, as detailed below.

As stated, the robot's outer cowl shown in Fig. 1 does not have enough waterproofing to prevent all raindrops from intruding from sensor clearances, so we prepared additional waterproofing and eaves produced by using 3D printers (Affinia H479, da Vinch 1.0).

Figure 4 shows CAD images of the eaves and expected raindrop flow lines on parts. Raindrops flow based on the arrows and do not enter sensor light receptors. The blowing of raindrops is blocked by these parts when wind is less than 3 m/s. When wind speed is 3 m/s, angles between an orthogonal line to the ground and the line which raindrops fall are from 25.1° to 27.7° [b]. These parts greatly reduce rain influence in sensor measurement. The effectiveness of these parts is discussed in the next section. Note that our navigation system as described here [2] does not depend on camera readings, and the robot's navigation function meets international protection waterproof standard X3 as detailed in Section 6.

Even if the blowing of raindrops is prevented, raindrops cannot be prevented from intruding when they rebound. For this reason, waterproof parts are installed at the inner cowl as shown in Fig. 5. Raindrops intruding into the robot fall onto the ground along to the parts, so water does

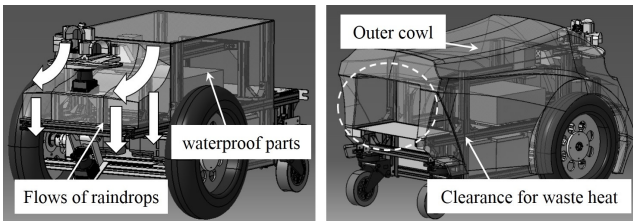


Fig. 5. Inner waterproof parts. Waste heat clearance is prepared behind the robot and is covered by the outer cowl for waterproofing purposes.

not pool in the cowl. Raindrops carried onto the cowl via wheel rotation are blocked by other waterproof parts forming a box (see Fig. 5). Since almost all electronic devices are placed in the box, so hardware problems due to water intrusion are prevented. These newly added parts enable the robot to work in strong rain.

4. Rain Influence on External Sensors

GPS, a camera, a RGB-D sensor, LIDAR, a magnetic sensor, and Wi-Fi are common external sensors (or systems) used in mobile navigation [10–15]. While GPS is commonly used in mobile navigation, using it for mobile robot navigation has not proven practical because multipaths cause fatal location estimate error which frequently occurs in outdoor environments. Its performance also depends on weather conditions [16]. A RGB-D sensor obtains camera images and depth data on the image simultaneously, but depth data cannot be obtained under strong sunlight. In other words, the RGB-D sensor performs similar to a camera in outdoor environments. To use a Wi-Fi-based method for mobile navigation, placing many access points is necessary to make Wi-Fi signal gradients which are used as landmarks. Many environmental arrange is necessary to achieve Wi-Fi based long-distance navigation.

Based on the above, we decided that a camera, LIDAR, and a magnetic sensor would be useful for investigating the influence of rain on these sensors.

4.1. Camera

Camera observation is blurred by raindrops getting on light receptors (Fig. 6) – a problem solved by the method proposed by Yamashita et al. using a pan-tilt camera [7]. Of course this method is effective, but we believe that a simpler method, e.g., a hardware mechanism such as a cover is needed to prevent the raindrop problems above.

Images in Fig. 6 were obtained in artificial rain. The figure at left was obtained with the waterproofing parts detailed in the previous section. Raindrops are prevented from getting on unwanted surfaces by these parts and thus helping to prevent adverse influences on images.

As shown in Fig. 4, raindrops cannot be prevented from getting on light receptors at an incidence angle from the ground under 60° . In cases such as this, a mechanical



Fig. 6. Raindrop influence on a camera image. The image at left was obtained when waterproofing parts were used. Raindrops did not become attached to light receptors, so measurement is clear. In contrast, the unclear figure at right was obtained when waterproofing parts were not used.

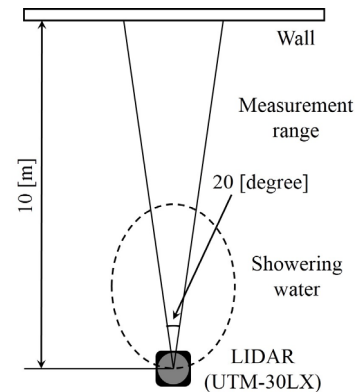


Fig. 7. Investigation condition for LIDAR readings.

function such as a wiper or similar to the method proposed by Yamashita et al. [7] is required, although implementing such techniques is difficult. To simply use a camera under rainy conditions, it should be tilted to the ground or covering it with eaves is preferable, but this restricts camera use. Our navigation system [2] does not use cameras, which means that the robot's navigation function is not influenced by camera observation, so we did not focus on ways to reduce the influence of rain on camera observation in this study.

4.2. LIDAR

We investigated how many raindrops were detected by LIDAR. We conducted this investigation under artificial rainy conditions using UTM-30LX as LIDAR. Fig. 7 shows the investigation scheme. We restricted the LIDAR measurement range so that its angle was only 20° . Water drops are showered in front of LIDAR using the hose in two cases, i.e., with and without eaves on the LIDAR and we counted detection number of water drops.

Table 1 lists the number of laser beams that hit water drops. In one investigation, 80 laser beams were output at 40 Hz for 5 seconds, i.e., 16,000 laser beams. Note that the cover reduced the number of water drops detected because water drops were prevented from getting on. Fig. 8 shows a histogram in which the bin size is set to 3 cm. It is obvious that the detection number of water drops in a short range of < 0.3 m is significantly reduced. From

Table 1. Number of laser beams hitting water drops. 80 laser beams were output at 40 Hz for 5 seconds, i.e., 16,000 laser beams were used in each investigation.

	1	2	3	4	5	Total	Average
Without the proof cover	148	225	302	210	173	1058	211.6
With the proof cover	69	69	115	98	89	440	88.0

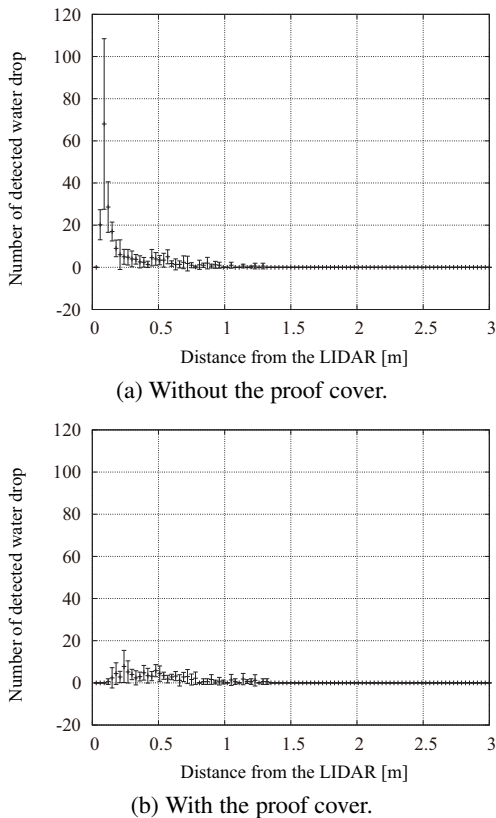


Fig. 8. Histogram of water drops detected by LIDAR.

these results, we considered that laser beams are reflected but that measurement could not be exact when water drops were attached to light receptors.

We further analyzed LIDAR readings when eaves was used. Water drops were 1 to 5 mm checked visually and 99.45% of the beams passed through this area (80,000 laser beams output and 440 laser beams hit water drops). This result might suggest that water drops be removed by ignoring small objects that suddenly appear. Fatal cases did occur, however, in which several beams detected water drops in a narrow area, e.g., as shown in **Fig. 9**, where six beams hit in a narrow area. Removing such influences must be done by focusing on size alone, removing objects 3 to 5 cm in size. This is not, however, suitable for obstacle avoidance, since this result shows that other types of raindrop removal are required.

4.3. Magnetic Sensor

Earth’s magnetic field depends on climate [17]. Climate change itself involves temperature and humidity

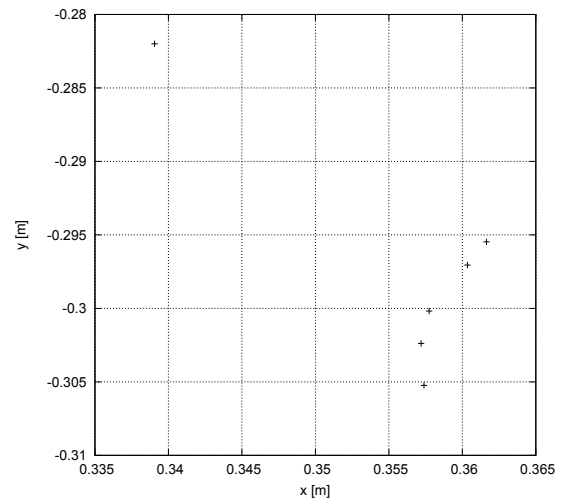


Fig. 9. Several beams detecting raindrops in a narrow area as they pass through an artificially rainy area.

changes – values influenced by rain. In contrast, the stability of magnetic fluctuations caused by magnetized materials such as steel frame and manholes against time progress has been reported [18]. We actually succeeded in long-distance navigation based on a localization method using magnetic fluctuation in actual outdoor environments [14] and showed the effectiveness of the localization method. We investigated how much influence due to environmental changes appears in magnetic sensor readings.

In our investigation here, we used the robot shown in **Fig. 1** to navigate the same straight path five times under different temperature and humidity conditions and recorded magnetic sensor readings at 40 Hz. Our objective in doing so was to develop mobile outdoor robots, so we focused only on outdoor magnetic fields.

The path we used includes magnetic fluctuations caused by magnetized materials. **Fig. 10** shows recorded results and each temperature and humidity values, denoted as $(T [C^{\circ}], H [%])$, were $(4, 75)$, $(5, 85)$, $(8, 45)$, $(8, 65)$, and $(19, 34)$. The magnetic sensor measures three axes, i.e., x , y , and z , magnetic intensities and azimuth angles. Where the xy plane is parallel to the ground and the directions of the x , y , and z axes face to a heading direction of the robot, right hand of the robot, and the ground. Note that state including travel distance of the robot was estimated by using the localization method described here [2] and we confirmed visually that estimated results are almost all correct.

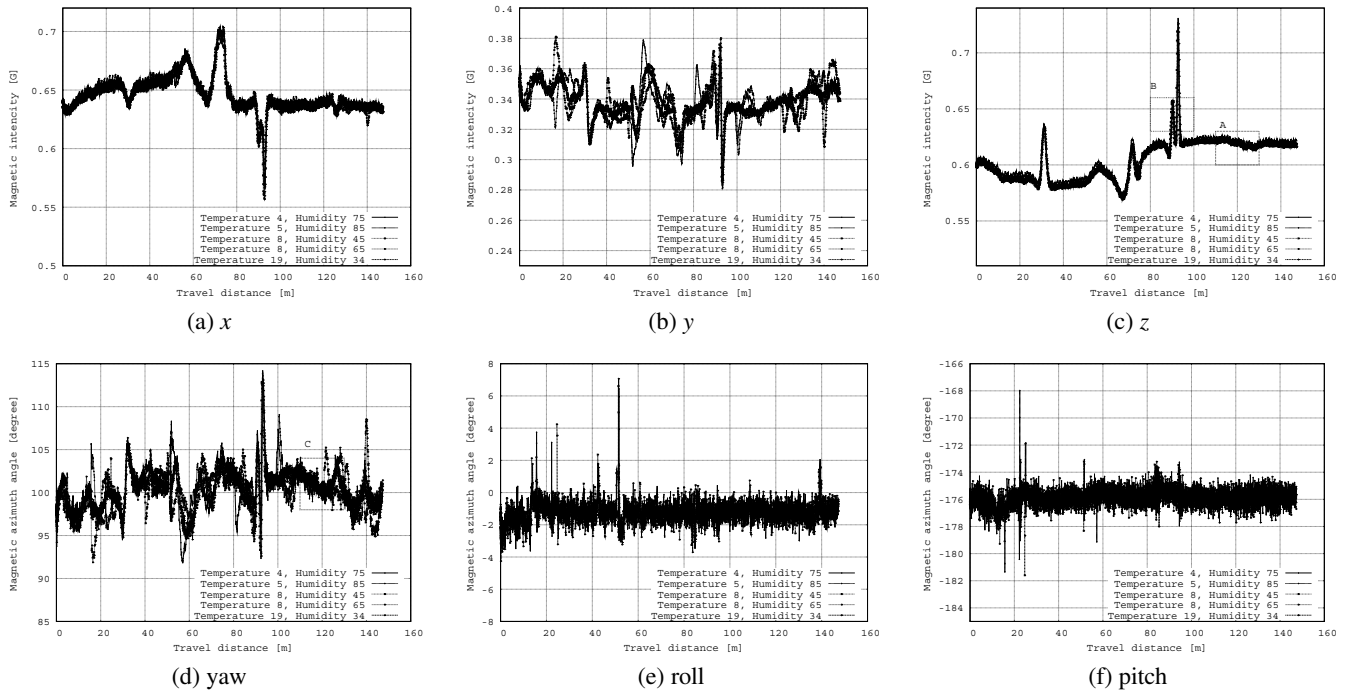


Fig. 10. Changes in magnetic sensor readings due to temperature and humidity changes on the same path. Figures at top show magnetic intensities – (a) is x , (b) is y , and (c) is z – and figures at bottom show magnetic azimuth angles – (d) is yaw, (e) roll, and (f) pitch.

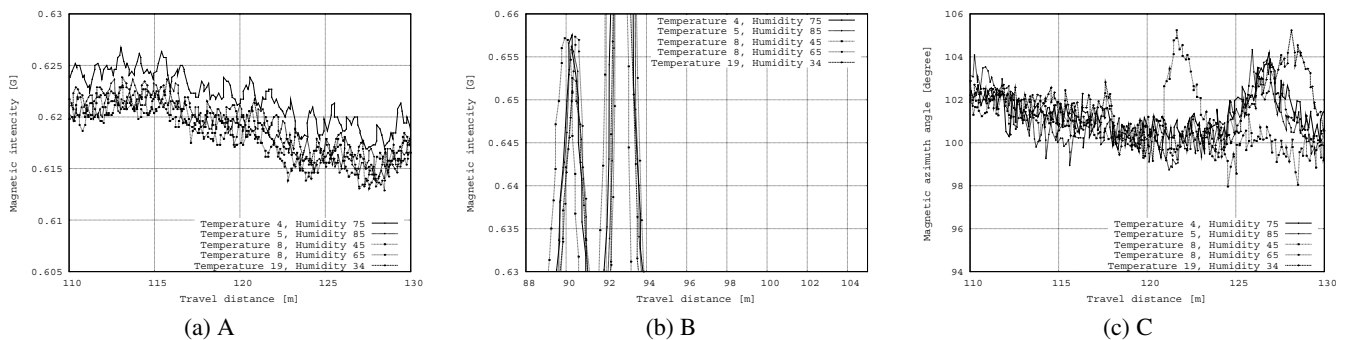


Fig. 11. Enlarged figures of part A, B, and C shown in Fig. 10.

This result shows that magnetic fluctuations are observed at the same positions and the same levels. **Figs. 11(a), (b), and (c)** show enlarged figures of part A, B, and C shown in **Fig. 10** (A and B are shown in **Fig. 10(c)** and C is shown in **Fig. 10(d)**). **Figs. 11(a)** and **(b)** show magnetic intensities of where a surrounding magnetic field does not contain and contain magnetic fluctuation. In both figures, changes in magnetic sensor readings due to temperature and humidity changes are confirmed. In contrast, however, the amplitude of magnetic fluctuation due to magnetized materials is enough larger than the change due to temperature and humidity changes. This indicates that magnetic fluctuation can be stably used as a landmark even if environmental changes occur.

Figure 11(c) shows magnetic azimuth angles of the yaw axis. Magnetic azimuth angles are often used in mobile navigation to estimate a heading direction, e.g., [19]. **Fig. 11(c)** indicates that the same magnetic azimuth angle

is measured in some areas even under different temperature and humidity conditions. Although it is not possible to use magnetic azimuth angles for estimating heading directions accurately in all areas, such estimation can be performed in some areas if accurate magnetic angles are selected. The localization method we proposed in a previous study [2] uses a magnetic azimuth angle and two threshold values to select accurate magnetic angles as detailed in Section 6. Its performance and effectiveness are shown through verification experiments.

5. Raindrop Detection from LIDAR Readings

From previous investigation, a fatal problem for autonomous navigation in rainy day appears in LIDAR readings. As we described before, the LIDAR detects raindrops as large objects more than its true size. This section

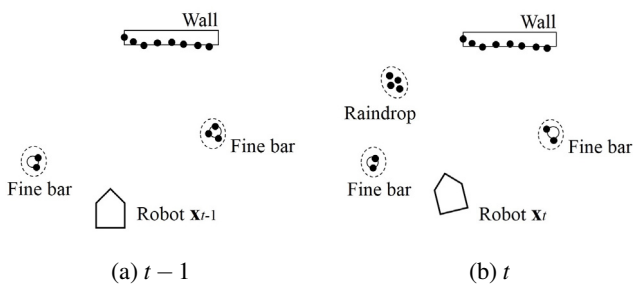


Fig. 12. Process for removing raindrops from LIDAR readings represented by black dots. Only small objects are detected from the readings and are recorded. Small objects detected from the current readings are compared with the recorded objects. If a detected object does not correspond to the past recorded objects, it is detected as raindrop.

describes how to remove raindrops from the LIDAR readings without removing other small objects.

Figure 12 shows a conceptual image of process to remove raindrops. The LIDAR readings are first clustered and a global position of small objects, whose cluster size is less than l , is recorded from time step $t - k - 1$ to $t - 1$. The global position is computed on the basis of the robot's localization result. Then a global 2D grid map, in which all initial values are set to 0, is defined and value of the grid, where the global positions exist, is incremented by using the all recorded data. In time step t , the current LIDAR readings are clustered again and the grid's value of a global position of small objects is checked. If the grid's value is less than n , the small object is detected as raindrop since it is regarded as a suddenly detected small object. If a detected small object is raindrop, it might appear suddenly and it can be detected by considering past LIDAR readings.

Figure 12 shows a case where k is 0. In implementation, l , k , and n are set to 10 cm, 10, and 4, respectively and grid size is set to 10 cm. Where computation cycle is 10 Hz.

6. Verification

6.1. Obstacle Avoidance

Figure 13 illustrates the outline of the obstacle avoidance method used in this verification. We briefly describe its overview in this section since this is detailed here [2].

First, LIDAR readings are plotted and a local obstacle map is constructed. LIDAR readings regarded as detecting raindrops are not used to construct the map. Next, calculate from the velocity command $\mathbf{u}_o = [v_o, \omega_o]$ the robot's travel paths and distances to the obstacles. The distances d to the obstacles are obtained by using velocity command \mathbf{u}_o , accumulating the robot's travels for every Δt second, and determining each time whether or not the robot may collide with the obstacles. If the robot's travel paths are found to lead to collision with the obsta-

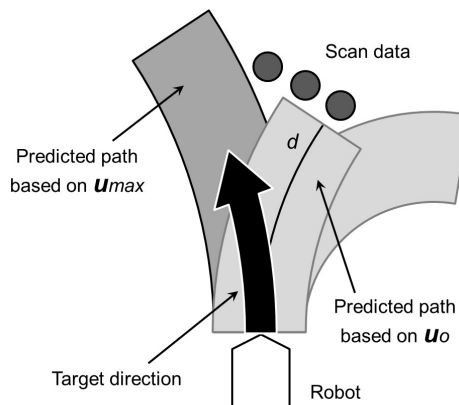


Fig. 13. Outline of the obstacle avoidance [2].

cles, velocity command \mathbf{u}_o is corrected as follows to make $\mathbf{u}_o = [v_o, \omega_o]$:

$$v_a = v_o(1 - K_v|\omega'|) \dots \dots \dots (1)$$

$$\omega_a = \omega_o + \omega' \dots \dots \dots (2)$$

where K_v denotes deceleration gains and ω' denotes corrected angular velocities. The corrected velocity command \mathbf{u}_a is used to recalculate the distances d_a between the robot's travel paths and the obstacles. Using the distances d_a , the evaluation value e_a for the corrected velocity command \mathbf{u}_a is defined as follows:

$$e_a = d_a \exp(-K_e \omega'^2) \dots \dots \dots (3)$$

To avoid some obstacles, the robot travels on the velocity command \mathbf{u}_{max} that gets the highest evaluation value e_a when the corrected angular velocity ω' changes little by little. If every d_a is less than a certain value, the robot judges that this is a situation in which the robot cannot avoid the obstacles and comes to a halt. If such a situation continues for a predetermined length time, the robot begins to retreat. In the actual implementations, with $K_v = 0.3$ and $K_e = 0.05$, ω' changes every 0.03 rad/s in the range of $-0.6 \leq \omega' \leq 0.6$ rad/s.

6.2. Magnetic Map-Based Heading Direction Estimate

The localization method that we proposed [2] uses a magnetic map which records a magnetic field on a travel path. In the magnetic map, magnetic intensity which goes to the ground m_z and magnetic azimuth angle which is parallel to the ground m_θ are recorded. In this study, direction for the ground is regarded as z direction and the magnetic angle is denoted as follows:

$$m_\theta = \theta + s_\theta, \dots \dots \dots (4)$$

where θ and s_θ denote heading direction of the robot and yaw angle measured by a magnetic sensor. The magnetic map is represented by a 2D grid map and only grids where the robot passed during map building phase record these magnetic data.

In the localization phase, the robot's state is first updated on the basis of odometry and the updated state is denoted as $\hat{\mathbf{x}} = (\hat{x}, \hat{y}, \hat{\theta})^T$. Two variables, r_z and r_θ , are then computed as follows:

$$r_z = 1 - \frac{|m_z - m_z(\hat{x}, \hat{y})|}{1}, \dots \dots \dots (5)$$

$$r_\theta = 1 - \frac{|m_\theta - m_\theta(\hat{x}, \hat{y})|}{\pi}, \dots \dots \dots (6)$$

where $m_z(\hat{x}, \hat{y})$ and $m_\theta(\hat{x}, \hat{y})$ are recorded values in the magnetic map. These values represent difference of current measurement and recorded values and it can be regarded that current and recorded magnetic fields are similar when these values close to 1. If these values exceed predetermined threshold values, heading direction is corrected as follows.

$$\theta = m_\theta(\hat{x}, \hat{y}) - s_\theta. \dots \dots \dots (7)$$

The threshold values, t_z and t_θ , were set to 0.994 and 0.992 experimentally.

The localization method is based on Monte Carlo Localization (MCL) [20] and this heading direction estimate is heuristically integrated into procedure of MCL. However, this is not detailed here because importance in this study is that whether heading direction estimate can be performed even if environmental condition changes.

6.3. Navigation in Rainy Situation

We conducted navigation experiments in the artificial rainy situation. In this environment, fine bars (tripod) are placed on a path which the robot has to trace. The diameter of the bars are 3 cm. Water drops are showered in front of the robot by using hose during the navigation.

Figure 14 shows a desired path and trajectories of the robot with and without the raindrop detection method. The trajectory without the raindrop detection method is smooth than the trajectory with the method. This is because that the raindrop detection method sometimes removes the fine bars and the robot cannot detect them from far areas (approximately 3 m). As a result, obstacle avoidance was not performed from far areas and the robot quickly avoided after it approaches to the object. In contrast, the robot could detect the bars from far areas when the method was not used and the trajectory was to be smooth. However, raindrops were detected many times when the method was not used and about 400 seconds were used to navigate this path. On the other hand, about 40 seconds were used to navigate this path when the method was used. This result shows that the raindrop detection method improved navigation function of the robot in rainy situations.

Figure 15 shows the LIDAR readings with and without the method and camera images when the readings were obtained. Raindrops were detected when the method was not used and the robot emergently stopped since obstacles appear in front of the robot. The detection method reduced influence of raindrops and allowed the robot to exactly perform navigation and obstacle avoidance.

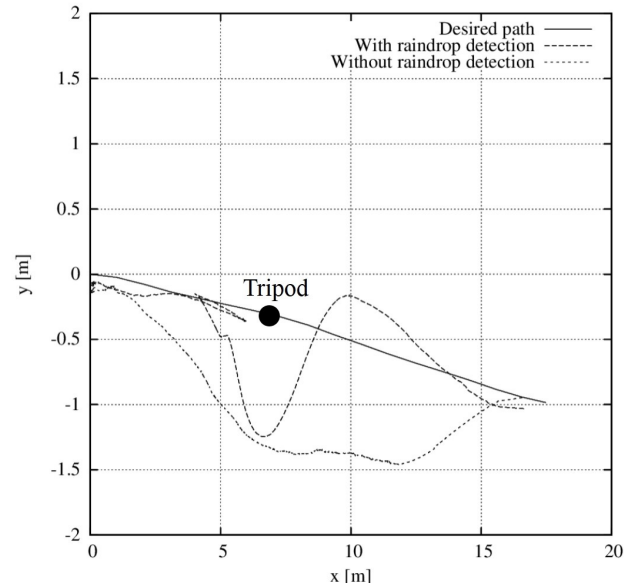
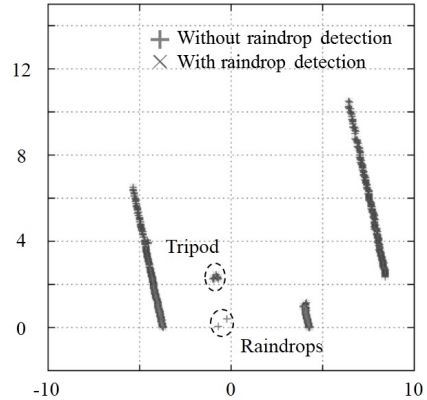
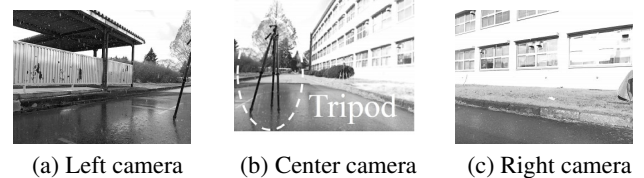


Fig. 14. Desired path and trajectories with and without the raindrop detection method.



(d) LIDAR readings used for obstacle avoidance

Fig. 15. Result of raindrop detection. Raindrop was removed by using the detection method.

However, the detection method has a problem that it cannot detect small objects that suddenly appear. This is because that these objects are distinguished as raindrops due to the algorithm. The fine bars cannot be always observed when the robot is far from the bar. By the reason, the fine bars were detected as raindrops when the robot observed from far areas. This may be a limit of the method and other device, e.g., camera, is needed to solve this problem.

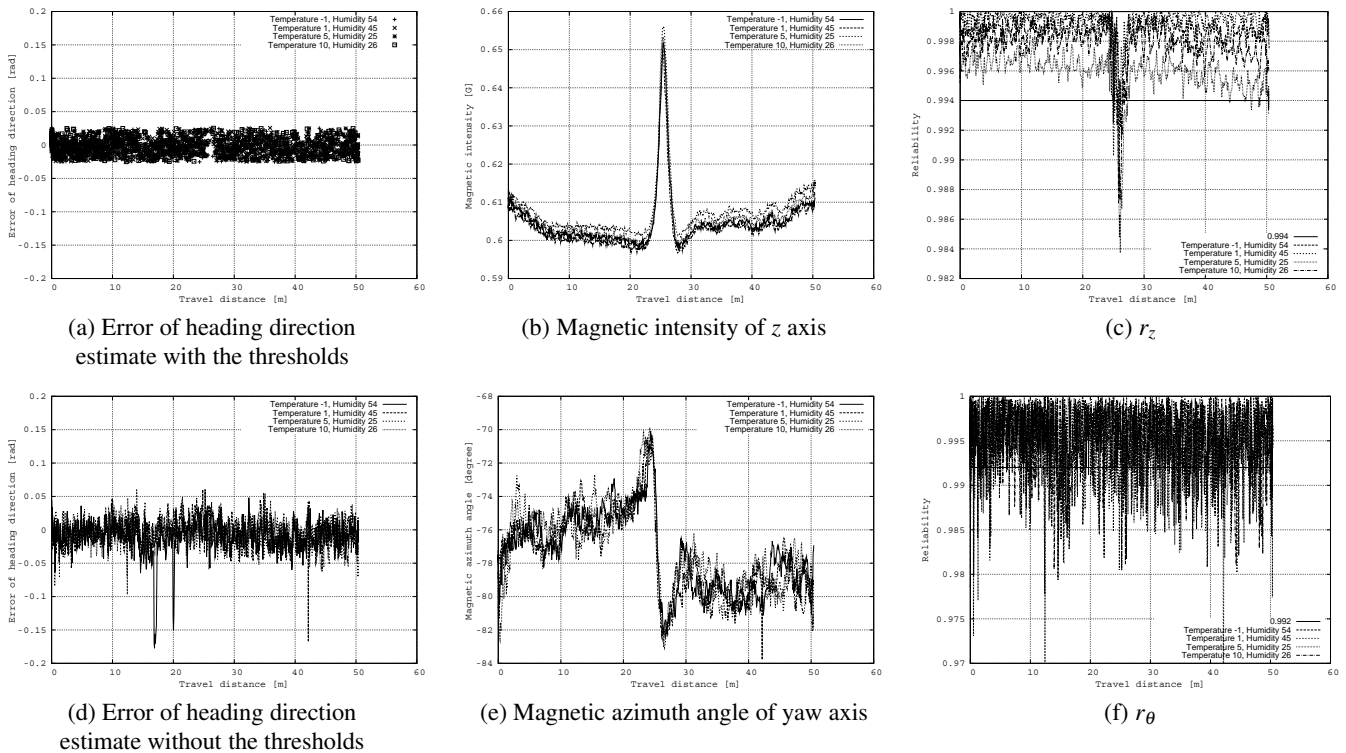


Fig. 16. Results of heading direction estimate.

6.4. Heading Direction Estimate

We conducted experiments of heading direction estimate in different temperature and humidity conditions like previous investigation for the magnetic sensor. In this experiment, we manually operated the robot on the travel path and recorded a result of heading direction estimate. The estimated result is compared with the geometric map-based localization result. We assumed that the geometric map-based localization result is ground truth since this experiments were conducted in an environment with enough geometric landmarks.

Figure 16(a) shows differences of estimated and ground truth heading directions. Also, Figs. 16(b) and (e) show magnetic intensity of z axis and magnetic azimuth angle of yaw axis and Figs. 16(c) and (f) show values of r_z and r_θ shown in Eqs. (5) and (6). Since heading direction estimate is only performed when the values exceed predetermined thresholds, difference of the directions are recorded discontinuously. Number of which heading direction estimate is performed changes due to the environmental conditions, but its accuracy is same in every experiment. Fig. 16(d) also shows errors of heading direction estimate when the threshold values are not used, namely heading direction estimate always performed. As can be seen in the figure, the errors became larger than the errors when the thresholds were used. This result shows that accurate magnetic angles can be selected by using the thresholds. As a result, performance of the threshold values were shown and effectiveness of using the magnetic map for localization was confirmed.

6.5. Waterproof Function

Through the above verifications, the robot stayed in the artificial rainy situations long time. Nevertheless, the robot worked and hardware problems did not occur. Numerically evaluating waterproof function is difficult, but we believe that this result shows enough waterproof function for the mobile outdoor robot and using 3D printers for producing additional eaves parts is useful to develop outdoor robots.

Japanese Industrial Standard (JIS) includes a standard for waterproof which is called International Protection X8 (IPX8). In the standard, a level, which prevents fatal problems when angles between an orthogonal line to the ground and a line which raindrops fall are under 15° , is defined as class 2. Also, a level, which prevents fatal problems when the angles are under 60° , is defined as class 3. Waterproof function of the robot is regarded as class 3 if we focus on only preventing hardware breakdown. However, raindrops attachment to the light receptors of the cameras cannot be prevented in a case where the angles exceed 30° . In this case, exact camera observation cannot be obtained. This means that waterproof function of the robot is regarded as class 2 on IPX8 when it executes person detection mission since this function is performed by using the cameras.

Since almost all robots have complex systems which is constructed by hardware and software layers, influence of rain appears in any level as we above mentioned. To develop outdoor robots, considering not only hardware breakdown but also any level waterproof function is needed. However, we consider that IPX8 may not con-

tain enough rule for such robots because IPX8 is not suitable standard for software level problem. Thus we consider that IPX8 is not suitable standard for outdoor robots and new standard has to be established for outdoor autonomous robot's waterproof.

6.6. Navigation in Actual Rainy Situation

We further conducted same navigation experiment in actual rainy situation. Almost all precipitation amounts when we conducted the experiment were approximately from 1 to 3 mm/h. There are no significant influence of rain to the navigation since precipitation amounts are extremely smaller than that of Tsukuba Challenge 2015 and our artificial rainy situation. Of course we do not frequently encounter strong rain like evening shower, but Tsukuba Challenge 2015 strongly showed us importance of considering influence of strong rain. We consider our study can provide contribution for such case.

7. Conclusion

In the Real World Robot Challenge (RWRC) 2015, every robot could not complete its mission. This is because that the RWRC 2015 was conducted in rainy day and the robots generated unexpected behavior since external sensors were influenced from the rain. The objective of this study was set to develop an autonomous mobile robot that can exactly navigate in rainy day.

We first described waterproof function for the robot used in this study. Almost all mobile robots are equipped with external sensors such as LIDARs or cameras for observing surroundings and clearances have to be prepared to place the sensors. Since raindrops intrude from the clearances and attach to light receptors of the sensors, we produced additional waterproof and eaves parts produced by using 3D printers. Using the 3D printers allowed us to flexibly design the parts and waterproof function of the robot could be improved. These parts reduced influence of rain against the sensors and prevented hardware problems of electronic devices.

We then investigated influence of rain against the camera, LIDAR, and magnetic sensor. Fatal influence appeared in the LIDAR readings since beams outputted from the LIDAR hit raindrops. We analyzed influence of rain against the LIDAR and described how to remove the raindrops from the readings. By considering past LIDAR readings, raindrops can be removed from the readings without removing other small objects, e.g., fine bars. Although small objects were sometimes detected as raindrops from far areas, obstacle avoidance against the objects was exactly performed since they could be detected in near areas.

We implemented above things to the robot developed by us in previous study and conducted navigation experiments in artificial rainy situations. Through the experiments, it was shown that autonomous navigation can be performed while reducing influence of rain.

This paper described how to remove raindrops from the LIDAR readings, but attachment of raindrops was not considered. This is because that we used eaves parts and assumed that the attachment can be prevented. However, the attachment might be happened in real world. Our future work is to consider it and solve this problem for practical navigation in rainy and snow situations and fuse LIDAR and camera readings for more accurately detecting raindrops.

Acknowledgements

This study was supported by KAKENHI 25420210. Moreover, NA received support from the late Dr. Saito. I would like to express my appreciation for his support and encouragement.

References:

- [1] S. Yuta et al., "Open experiment of autonomous navigation of mobile robots in the city: Tsukuba Challenge 2014 and the results," *J. of Robotics and Mechatronics*, Vol.27, No.4, pp. 318-326, 2015.
- [2] N. Akai et al., "Autonomous navigation based on magnetic and geometric landmarks on environmental structure in real world," *J. of Robotics and Mechatronics*, Vol.26, No.2, pp. 158-165, 2014.
- [3] N. Akai et al., "Development of mobile robot 'SARA' that completed mission in real world robot challenge 2014," *J. of Robotics and Mechatronics*, Vol.27, No.4, pp. 327-336, 2015.
- [4] K. Kaneko et al., "Humanoid robot HRP-3," *IEEE/RSJ Int. Con. on Intelligent Robots and Systems*, pp. 2471-2478, 2008.
- [5] K. Tanigaki et al., "Cherry-harvesting robot," *Computers and Electronics in Agriculture*, Vol.63, No.1, pp. 65-72, 2008.
- [6] G. Freitas et al., "Kinematic reconfigurability control for an environmental mobile robot operating in the Amazon rain forest," *J. of Field Robotics*, Vol.27, No.2, pp. 197-216, 2010.
- [7] A. Yamashita et al., "A virtual wiper - Restoration of deteriorated images by using a pan-tilt camera -," *IEEE Int. Conf. on Robotics and Automation*, pp. 4724-4729, 2004.
- [8] T. Fujisawa et al., "Correction methods for underwater scan data measured by general-purpose laser range finders," *Trans. of the Japan Society of Mechanical Engineering*, Vol.81, No.831, p. 15-00412, 2015 (in Japanese).
- [9] R. P. Gorman et al., "Analysis of hidden units in a layered network trained to classify sonar targets," *Neural Networks*, Vol.1, No.1, pp. 75-89, 2002.
- [10] T. Suzuki et al., "Autonomous navigation of a mobile robot based on GNSS/DR integration in outdoor environments," *J. of Robotics and Mechatronics*, Vol.26, No.2, pp. 214-224, 2014.
- [11] K. Irie et al., "Outdoor localization using stereo vision under various illumination conditions," *Advanced Robotics*, Vol.26, No.3-4, pp. 327-348, 2012.
- [12] J. Biswas et al., "Depth camera based indoor mobile robot localization and navigation," *IEEE Int. Conf. on Robotics and Automation*, pp. 1697-1702, 2012.
- [13] T. Yoshida et al., "A sensor platform for outdoor navigation using gyro-assisted odometry and roundly-swinging 3D laser scanner," *IEEE/RSJ Int. Conf. on Intelligent Robots and Systems*, pp. 1414-1420, 2010.
- [14] S. A. Rahok et al., "Navigation using an environmental magnetic field for outdoor autonomous mobile robots," *Advanced Robotics*, Vol.26, No.3-4, pp. 1751-1771, 2011.
- [15] J. Biswas et al., "Wifi localization and navigation for autonomous indoor mobile robots," *IEEE Int. Conf. on Robotics and Automation*, pp. 4379-4384, 2010.
- [16] D. Dong et al., "Anatomy of apparent seasonal variations from GPS-derived site position time series," *J. of Geophysical Research*, Vol.107, No.B4, 2002.
- [17] V. Courtillot et al., "Are there connections between the Earth's magnetic field and climate?" *Earth and Planetary Science Letters*, Vol.253, No.3-4, pp. 328-339, 2007.
- [18] K. Yamazaki et al., "Analysis of magnetic disturbance due to buildings," *IEEE Trans. on Magnetics*, Vol.25, pp. 4006-4008, 1989.
- [19] W. Kwon et al., "Particle filter-based heading estimation using magnetic compasses for mobile robot navigation," *IEEE Int. Conf. on Robotics and Automation*, pp. 2705-2712, 2006.

- [20] F. Dellaert et al., "Monte Carlo localization for mobile robots," IEEE Int. Conf. on Robotics and Automation, Vol.2, pp. 1322-1328, 1999.

Supporting Online Materials:

- [a] <http://www.greenlife-web.co.jp/>
(in Japanese) [Accessed August 2, 2016]
[b] <http://www.s-yamaga.jp/nanimono/taikitoumi/amenoseiin.htm>
(in Japanese) [Accessed August 2, 2016]



Name:
Naoki Akai

Affiliation:
Institutes of Innovation for Future Society,
Nagoya University

Address:

Furo, Chikusa, Nagoya, Aichi 464-8601, Japan

Brief Biographical History:

2013-2016 Doctor Student, Utsunomiya University

2016- Designated Assistance Professor, Nagoya University

Main Works:

- "Development of mobile robot 'SARA' that completed mission in real world robot challenge 2014," J. of Robotics and Mechatronics, Vol.27, No.4, pp. 327-336, 2015.
- "Gaussian processes for magnetic map-based localization in large-scale indoor environments," IEEE/RSJ Int. Conf. on Intelligent Robots and Systems, pp. 4459-4464, 2015.

Membership in Academic Societies:

- The Japan Society of Mechanical Engineers (JSME)
- The Robotics Society of Japan (RSJ)
- The Society of Instrument and Control Engineers (SICE)



Name:
Yasunari Kakigi

Affiliation:
Graduate School of Engineering, Utsunomiya
University

Address:

7-1-2 Yoto, Utsunomiya-shi, Tochigi 321-8585, Japan

Brief Biographical History:

2015- Master Student, Utsunomiya University

Main Works:

- "Appearance design for mobile robots with functions," The 15th SICE System Integration Division Annual Conf. Proc., 1F3-3, 2014 (in Japanese).

Membership in Academic Societies:

- The Robotics Society of Japan (RSJ)



Name:
Shogo Yoneyama

Affiliation:
Graduate School of Engineering, Utsunomiya
University

Address:

7-1-2 Yoto, Utsunomiya-shi, Tochigi 321-8585, Japan

Brief Biographical History:

2015- Master Student, Utsunomiya University

Main Works:

- "Task simplification in the tsukuba challenge and navigation strategy," The 16th SICE System Integration Division Annual Conf. Proc., 1K4-6, 2015 (in Japanese).



Name:
Koichi Ozaki

Affiliation:
Graduate School of Engineering, Utsunomiya
University

Address:

7-1-2 Yoto, Utsunomiya-shi, Tochigi 321-8585, Japan

Brief Biographical History:

1996-2003 Assistance Professor, Utsunomiya University

2003-2010 Associate Professor, Utsunomiya University

2011- Professor, Graduate School of Engineering, Utsunomiya University

Main Works:

- "Application of localization based on DC magnetic field occurred in the environment on wheel type mobile agriculture robots," Advanced Robotics, Vol.25, No.3, pp. 923-939, 2011.

Membership in Academic Societies:

- The Japan Society of Mechanical Engineers (JSME)
- The Robotics Society of Japan (RSJ)
- The Japan Society of Kansei Engineering (JSKE)